On the response of the Antarctic Circumpolar Current transport to climate change in coupled climate models

On the response of the Antarctic Circumpolar Current transport to climate change in coupled climate models

Z. Wang,[1] T. Kuhlbrodt,[2] and M. P. Meredith[1]

Received 22 October 2010; revised 24 March 2011; accepted 12 May 2011; published 10 August 2011.

[1] The Coupled Model Intercomparison Project phase 3 (Intergovernmental Panel on Climate Change (IPCC) Fourth Assessment Report) models show a consistent intensification and poleward shift of the westerly winds over the Southern Ocean during the 21st century. However, the responses of the Antarctic Circumpolar Currents (ACC) show great diversity in these models, with many even showing reductions in transport. To obtain some understanding of diverse responses in the ACC transport, we investigate both external atmospheric and internal oceanic processes that control the ACC transport responses in these models. While the strengthened westerlies act to increase the tilt of isopycnal surfaces and hence the ACC transport through Ekman pumping effects, the associated changes in buoyancy forcing generally tend to reduce the surface meridional density gradient. The steepening of isopycnal surfaces induced by increased wind forcing leads to enhanced (parameterized) eddy-induced transports that act to reduce the isopycnal slopes. There is also considerable narrowing of the ACC that tends to reduce the ACC transport, caused mainly by the poleward shifts of the subtropical gyres and to a lesser extent by the equatorward expansions of the subpolar gyres in some models. If the combined effect of these retarding processes is larger than that of enhanced Ekman pumping, the ACC transport will be reduced. In addition, the effect of Ekman pumping on the ACC is reduced in weakly stratified models. These findings give insight into the reliability of IPCC-class model predictions of the Southern Ocean circulation and into the observed decadal scale steady ACC transport.

Citation: Wang, Z., T. Kuhlbrodt, and M. P. Meredith (2011), On the response of the Antarctic Circumpolar Current transport to climate change in coupled climate models, *J. Geophys. Res.*, *116*, C08011, doi:10.1029/2010JC006757.

1. Introduction

[2] Changes in the Southern Ocean (SO) circulation are important because of their impacts on global meridional overturning circulation (MOC), heat uptake, and the global carbon budget [e.g., *Toggweiler and Samuels*, 1995; *Sabine et al.*, 2004; *Stouffer et al.*, 2006; *Le Quéré et al.*, 2007]. The Antarctic Circumpolar Current (ACC) is a critical component in the SO circulation, being closely coupled to the SO overturning circulation [*Marshall and Radko*, 2003], the subtropical gyres to the north and the subpolar gyres to the south. Responses of the ACC to changes in atmospheric forcing are thus of central concern in climate change studies. A large number of observational studies [e.g., *Rintoul and Sokolov*, 2001; *Aoki*, 2002; *Hughes et al.*, 2003; *Meredith et al.*, 2004; *Böning et al.*, 2008] and modeling studies [e.g., *Hall and Visbeck*, 2002; *Bi et al.*, 2002; *Oke and England*, 2004; *Saenko et al.*, 2005; *Fyfe and Saenko*, 2006; *Sen Gupta and England*, 2006; *Hallberg and Gnanadesikan*, 2006; *Meredith and Hogg*, 2006] have addressed the sensitivity of the ACC to atmospheric forcing changes. Many of the previous modeling studies have used coarse-resolution ocean models, and have shown that the simulated ACC intensifies in response to the strengthening of the westerlies over the SO [e.g., *Hall and Visbeck*, 2002; *Bi et al.*, 2002; *Oke and England*, 2004; *Saenko et al.*, 2005; *Fyfe and Saenko*, 2006; *Sen Gupta and England*, 2006]. However, as more results became available, it was found that the changes in the ACC transport in response to the strengthening of the westerlies vary considerably among the Intergovernmental Panel on Climate Change (IPCC) Fourth Assessment Report (AR4) coupled climate models, to the extent of there being significant reductions of the ACC transport in some models [see *Sen Gupta et al.*, 2009]. In this study, we examine the large-scale forcings and mechanisms responsible for these ACC changes, with a focus on understanding the diverse responses of the ACC transport in these models.

[3] Observational studies have shown that the ACC transport varies on timescales from days to years [*Aoki*, 2002; *Hughes et al.*, 2003; *Meredith et al.*, 2004], in response to the

[1]British Antarctic Survey, Cambridge, UK.
[2]Department of Meteorology, NCAS-Climate, University of Reading, Reading, UK.

0148-0227/11/2010JC006757

Table 1. Nineteen IPCC AR4 Coupled Climate Models Used in This Study

Model Number	Model Name	Country	Resolution (x; y; z)	Eddy Parameterization[a]
1	cccma_cgcm3_1	Canada	1.875°; 1.875°; 29 levels	GM90
2	cccma_cgcm3_1_t63	Canada	1.4°; 0.94°; 29 levels	GM90
3	cnrm_cm3_0	France	2°; 1.5°–0.5°; 31 levels	GM90
4	csiro_mk3_0	Australia	1.87°; 0.84°; 31 levels	GM90, Griffies98
5	csiro_mk3_5	Australia	1.87°; 0.84°; 31 levels	GM90, Griffies98
6	gfdl_cm2_0	USA	1°; 1°–0.33°; 50 levels	Griffies98, Griffies05
7	gfdl_cm2_1	USA	1°; 1°–0.33°; 50 levels	Griffies98, Griffies05
8	giss_aom	USA	4°; 3°; 16 levels	none
9	giss_model_e_r	USA	5°; 4°; 13 levels	Visbeck97, Griffies98
10	ingv_echam4	Italy	2°; 2°–1°; 33 levels	Treguier97
11	ipsl_cm4	France	2°; 2°–1°; 31 levels	Treguier97
12	miroc3_2_hires	Japan	0.28°; 0.19°; 47 levels	Gent95
13	miroc3_2_medres	Japan	1.4°; 1.4°–0.56°;43 levels	Gent95
14	miub_echo_g	Germany/Korea	2.8125°; 2.79°–0.5°; 20 levels	none
15	mpi_echam5	Germany	1.5°; 1.5°; 40 levels	Gent95, Griffies98
16	mri_cgcm2_3_2a	Japan	2.5°; 2°–0.5°; 23 levels	GM90
17	ncar_ccsm3_0	USA	1.125°; 0.53°–0.27° y; 40 levels	GM90, Griffies98
18	ncar_pcm1	USA	1.125°; 0.53°–0.27°; 40 levels	GM90, Griffies98
19	ukmo_hadcm3	UK	1.25°; 1.25°; 20 levels	Gent95, Visbeck97, Wright97

[a]The relevant references for GM90, Gent95, Griffies98, Griffies05, Treguier97, Visbeck97, and Wright97 are *Gent and McWilliams* [1990], *Gent et al.* [1995], *Griffies* [1998], *Griffies et al.* [2005], *Treguier et al.* [1997], *Visbeck et al.* [1997], and *Wright* [1997], respectively.

variability of the westerly winds over the SO. The variability of the ACC transport is rather small, however, changing peak to peak by only around 7 Sv (5% of its mean) on interannual timescales despite much larger relative changes in the overlying wind field [*Meredith et al.*, 2004]. On decadal timescales, the analysis of hydrographic data by *Böning et al.* [2008] suggested that the ACC transport has changed little during the past several decades, despite large increases of the westerlies over the SO. One process that has been proposed as a mechanism to explain this weak response of the ACC transport is the intensification of the SO eddy field on interannual timescales, cascading energy from the mean flow to the ocean mesoscale [*Hallberg and Gnanadesikan*, 2006; *Meredith and Hogg*, 2006; *Böning et al.*, 2008].

[4] Over the SO, the prevailing eastward wind stress transfers the eastward momentum into the ocean and drives the northward Ekman transport across the ACC. The convergence of the Ekman transport on the northern side of the ACC leads to downwelling there, and the divergence leads to the upwelling on the southern side. The large eastward current is thus maintained through the geostrophic balance with the tilted isopycnal structure driven by Ekman pumping combining with buoyancy forcing. However, it is a very difficult challenge to predict the change in the ACC transport, because a number of other important processes also need to be taken into account, including ocean stratification, eddy transports, and the dynamic effects of topography [*Rintoul et al.*, 2001; *Olbers et al.*, 2004].

[5] Not all of these processes could be analyzed here due to the lack of data or insufficient data quality in the archives of IPCC AR4 model results. This concerns quantifying the impacts of the parameterized eddy-induced transports in particular. Nevertheless, the analysis of the changes in major large-scale processes, such as wind stress, surface density flux, isopycnal structure and implied associated eddy-induced transport, and the pattern of ocean zonal transport, that we present here can nonetheless reveal mechanisms in the models that explain the varying ACC transport responses, and particularly the simulated slowdown of the ACC in a number of the models.

[6] In the following, the models and data used are described in section 2. The projected trends of the ACC transports through Drake Passage over the 21st century are presented in Section 3, along with the corresponding trends of the Southern Annular Mode (SAM) indices. In section 4, we analyze the projected horizontal structures of changes in the momentum forcing and buoyancy forcing. The links between the ACC trends and the changes in wind and buoyancy forcing are investigated in section 5. We examine the detailed structures of the ACC changes and analyze the major large-scale processes that contribute to retarding the ACC in section 6. Concluding remarks are given in Section 7. Detailed analysis of internal drifts in the ACC transport is presented in Appendix A.

2. Models and Data

[7] The model data used are the output from 19 IPCC AR4 climate models. These models are listed in Table 1, along with their horizontal and vertical resolutions, and the eddy parameterizations used in the models. The detailed descriptions of these models can be found at http://www-pcmdi.llnl.gov/ipcc/model_documentation/ipcc_model_documentation.php.

[8] The horizontal resolutions of the ocean components of these models vary from very coarse resolutions (as in the two GISS models, models 8 and 9) to high resolution (eddy permitting, model 12). Generally, the horizontal grid sizes are about 1 or 2 degrees. Most models employ a z coordinate, except for the two GISS models that use a fixed number of levels with a fixed proportion of mass in the column, and the two Japanese models that use hybrid z and sigma coordinates, with the vertical resolutions varying from 13 levels in model 9 to 50 levels in several models. The *Gent and McWilliams* [1990] (GM90) parameterization, or forms developed from it [*Gent et al.*, 1995; *Treguier et al.*, 1997; *Visbeck et al.*, 1997; *Wright*, 1997; *Griffies*, 1998; *Griffies et al.*, 2005], are used to represent the eddy-induced tracer transports in most models.

[9] Here, we mainly use the output from runs with one greenhouse gas emission scenario, namely SRESA1B (see *Intergovernmental Panel on Climate Change* (*IPCC*) [2001,

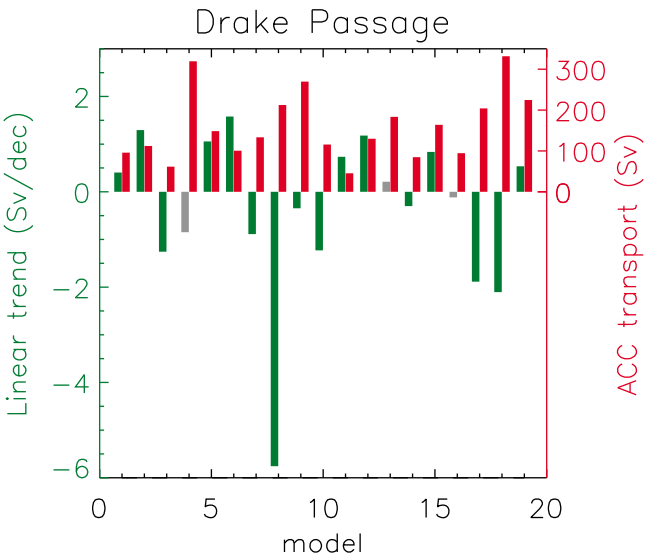

Figure 1. Linear trends (green and grey, left axis) in the total ACC transports through Drake Passage over the 21st century, and the mean transports over 2001–2010 (red, right axis) for the 19 models. The trends in grey are not statistically significant at the 5% level. The observed estimates of the ACC transport through Drake Passage is about 135 Sv [e.g., *Cunningham et al.*, 2003].

Appendix II] for the details of this scenario), in which CO_2 is increased from the present-day level to 703 ppm at the end of the 21st century. Output from preindustrial runs and commit runs (major GHG concentrations kept constant through the 21st century at their values from the end of the 20th century) are also examined, to check the magnitudes of the ACC drifts in unforced runs (see Appendix A).

[10] The linear trends are derived from the slopes of best linear fits (least squares) to the time series of the annual means of relevant variables over the 21st century. The *t* test is performed for determining the significance of the trends.

3. Projected Trends in ACC Transport and SAM Index Over the 21st Century

3.1. Trends in ACC Transport

[11] In the following we calculate and present the ACC trends over the 21st century. While some models have runs that extend beyond this time frame, a full intercomparison requires a common temporal domain. Figure 1 shows the linear trends of the total ACC transports through Drake Passage over the 21st century for the 19 models. There is a very large intermodel spread, with trends ranging from −5.76 Sv decade^{-1} for model 8 to 1.58 Sv decade^{-1} for model 6. The multimodel ensemble mean is −0.36 Sv decade^{-1}, and the intermodel standard deviation is 1.70 Sv decade^{-1}. Figure 1 indicates that many of the IPCC AR4 models predict decelerations of the ACC over the 21st century, and the multimodel ensemble also predicts a weakening, albeit a small one (much smaller than the intermodel standard deviation). A comparison with the trends in the preindustrial runs and the commit runs is given in Appendix A.

3.2. Trends in the Southern Annular Mode

[12] Many previous studies have investigated the atmospheric forcing of SO circulation changes via quantification of a SAM index. Following *Gong and Wang* [1999] and *Marshall* [2003], the SAM index is calculated here as the zonal mean of sea level pressure at 40S minus that at 65S. The trends of SAM index are shown in Figure 2, along with the averaged SAM indices over the first decade of the 21st century. There is a very large intermodel spread for both the trends and the averaged SAM indices. The trends range from −15.8 Pa decade^{-1} for model 18 to 55.3 Pa decade^{-1} for model 14. The multimodel ensemble mean is 35.2 Pa decade^{-1}, and the intermodel standard deviation is 24.2 Pa decade^{-1}. The ensemble mean of the SAM index trends is significantly positive and comparatively much larger than that of ACC transport trends. (The change in the ensemble mean SAM index over the century is 12%, while it is just −2.3% for the change in the ACC transport.) Although the intermodel spread of SAM index trends is very large, almost all the models have positive trends over the 21st century, except for model 18. This particular model has a negative trend, because the response to the recovery of the ozone hole is dominant over the effect of greenhouse gas increases, as discussed by *Miller et al.* [2006].

[13] There are also some other notable features in Figure 2, for example the large trend in model 14 compared with the very small trends in the other models (models 4, 5, 8, 10, 17, and 19). By simply comparing Figure 2 with Figure 1 (see also a direct comparison in Figure 6), we see that the positive trends in the SAM index (increased westerlies) do not necessarily cause increases in the ACC transport. This is seen most clearly in model 14, where the largest increase in the westerlies corresponds to a significant negative ACC transport trend.

[14] Overall, the ACC transport responses to the increases in the westerlies are not consistent in these models. (We note that *Fyfe and Saenko* [2006] analyzed a subset of the models

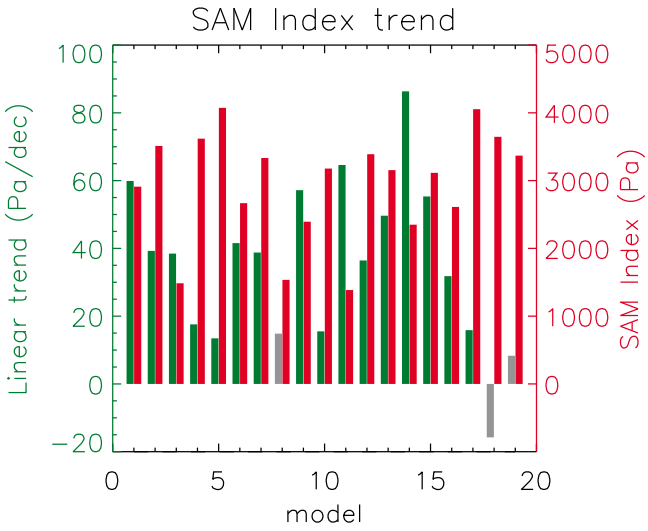

Figure 2. Linear trends in SAM index (see text for definition) over the 21st century (green and grey, left axis), and the mean SAM indices over 2001–2010 (red, right axis). The trends in grey are not statistically significant at the 5% level.

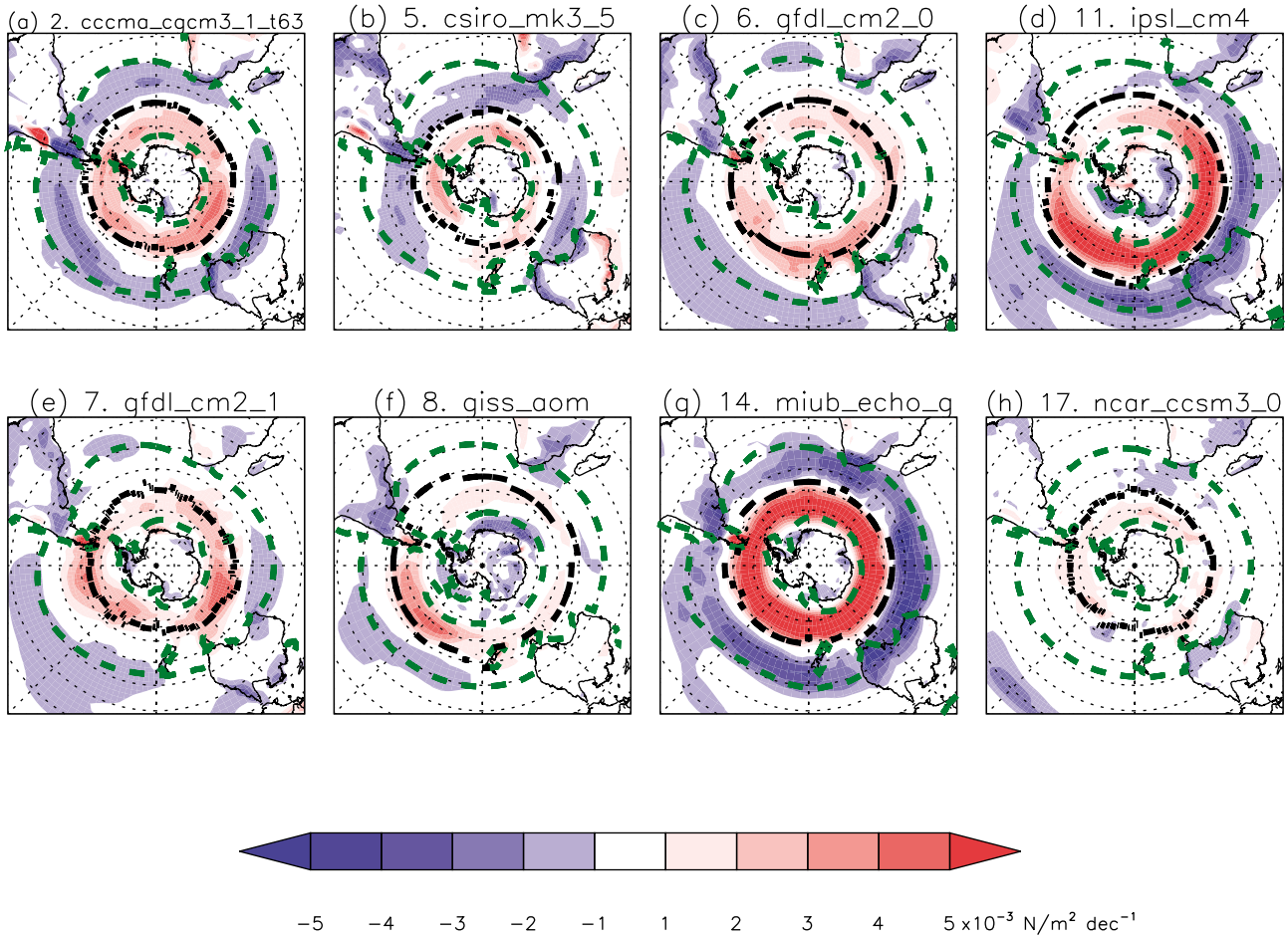

Figure 3. Linear trends in zonal wind stress over the 21st century for the eight selected models. Note that the significance level is not shown for the sake of clarity. The trends are generally statistically significant at the 5% significance level, if they are not very small. The dashed green lines mark the northern and southern boundaries of the westerlies averaged over the first decade of the 21st century, and the dashed black lines mark the locations of the maximum westerly wind.

used here, and observed more consistency in the ACC responses to SAM changes. However, their focus was on peak velocities, whereas ours is on transport.) In particular, in many cases there is a seemingly counterintuitive weakening of the ACC transport coincident with strengthening winds. In order to investigate this, we first examine changes in the momentum forcing and buoyancy in the models over the 21st century.

4. Changes in Momentum and Buoyancy Forcing Over the 21st Century

[15] In this section, we analyze changes in momentum and buoyancy forcing in eight selected models. All these models have positive SAM index trends, but four of them (models 2, 5, 6, and 11) have positive ACC transport trends, while the other four models (models 7, 8, 14 and 17) have negative ACC transport trends.

4.1. Changes in Zonal Wind Stress and Wind Stress Curl

[16] Figure 3 shows the trends of zonal wind stress over the 21st century for the 8 models selected, with Figures 3a–3d being models with a coincident positive ACC transport trend, and Figures 3e–3h being those with a negative ACC trend. The dashed green lines mark the northern and southern boundaries of the westerlies averaged over the first decade of the 21st century, and the dashed black lines mark the latitudes of the maximum westerly wind. Generally, the positive trends are quasi-circumpolar, with some local intensifications at various locations. The positive trends lie consistently to the south of the maximum westerly winds among these models, reflecting the poleward shifts of the westerlies. At and to the south of the northern boundaries, the trends are negative, indicating the broad poleward shifts of westerlies (and hence subtropical highs) in these models. Generally, the negative trends around the coast of the Antarctica are relatively small, with the exceptions of models 8 (Figure 3f) and 11 (Figure 3d). It is interesting to note that the westerly wind increase over the latitude band of Drake Passage is extremely large in model 14 (which has a negative trend of ACC transport through Drake Passage), while for model 11 (with a positive ACC trend) the largest increase of westerlies lies to the north of this latitude band, and that these two models have quite similar resolutions.

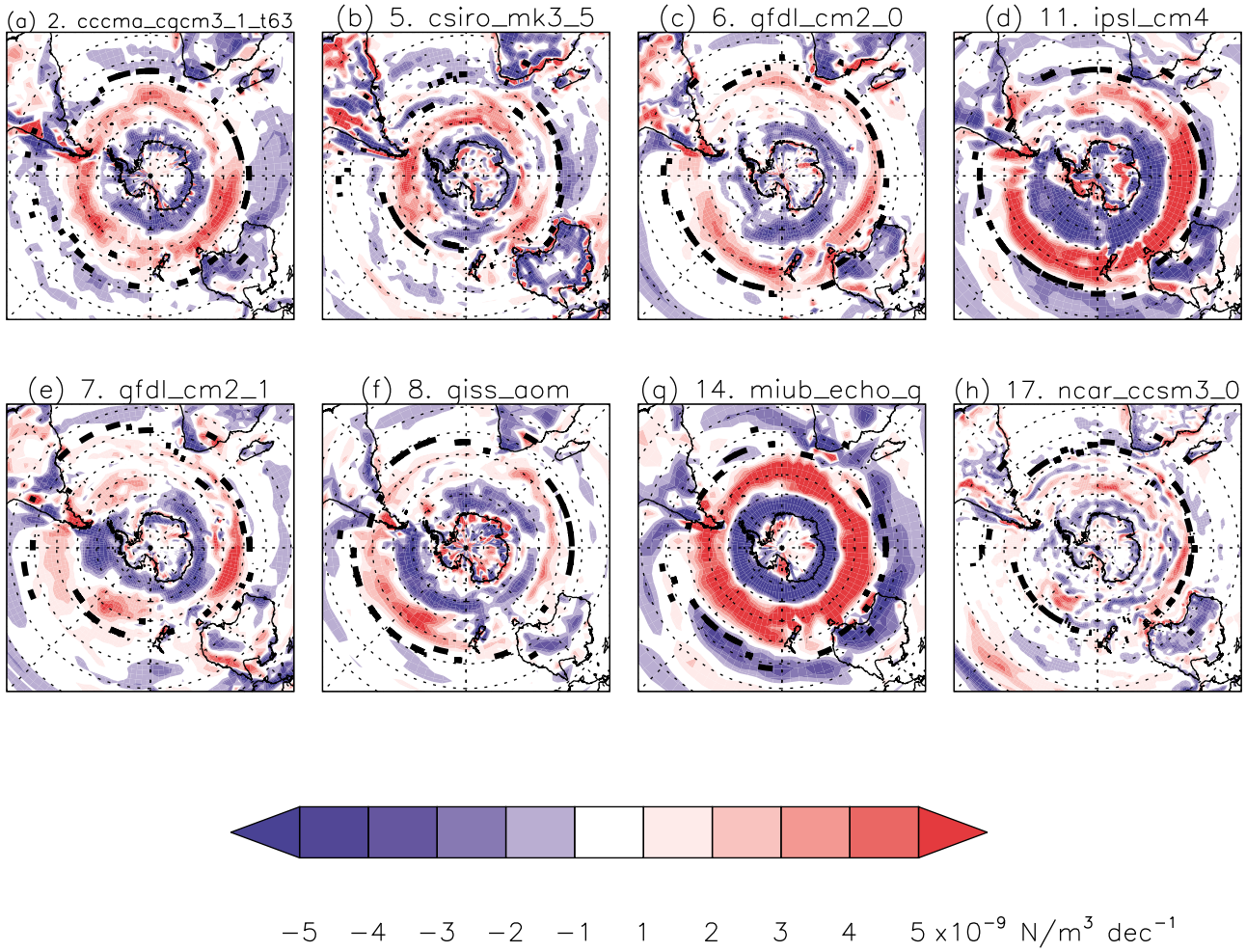

Figure 4. Linear trends in wind stress curl over the 21st century for the eight selected models. The dashed black lines mark the locations of maximum wind stress curl averaged over the first decade of the 21st century.

[17] Figure 4 show the trends of wind stress curl. The dashed black lines mark the latitudes of maximum positive wind stress curl averaged over the first decade of the 21st century, where the downward Ekman pumping velocities are the largest. The trends of wind stress curl are inevitably noisier than those of wind stress, however a robust feature is that the changes in wind stress curl are large for those models with large changes in zonal wind stress (Figure 4, cf. Figure 3). Generally, the wind stress curl increases (more anticyclonic wind forcing and more downward Ekman pumping) just to the south of the maximum wind stress curl averaged over the first 10 years, and the wind stress curl decreases at lower latitudes (less anticyclonic wind forcing) and in the subpolar region (more cyclonic wind forcing). There are considerable poleward shifts of the maximum positive wind stress curl, consistent with the findings of *Cai et al.* [2005], *Saenko et al.* [2005], and *Sen Gupta et al.* [2009].

4.2. Changes in Buoyancy Forcing

[18] Following *Large and Nurser* [2001], the density flux is calculated here as a function of net oceanic heat flux and freshwater flux, with positive values denoting the ocean surface losing buoyancy and hence becoming denser. Since there are no freshwater flux data available for some models, we use precipitation minus evaporation (P-E) instead along with net oceanic heat flux to calculate the density flux. For those models with both P-E data and freshwater flux data, the results obtained using P-E data agree well with those obtained using freshwater flux data. The only obvious difference is due to the sea ice retreat effects around the sea ice margins, which cause very narrow bands of positive density flux trends there. These positive trends in density flux are generally compensated by the small negative trends over a broader area at higher latitudes in these Coupled Model Intercomparison Project phase 3 (CMIP3) models. (Note that in the SO with negligible runoff, the freshwater flux is determined by P-E induced by atmospheric moisture transport and the melting/freezing of sea ice.)

[19] Figure 5 shows that there are general negative trends of density fluxes (that tend to make the surface water lighter) at higher latitudes in these eight models, except in model 11. This is generally because of increased heat input to the

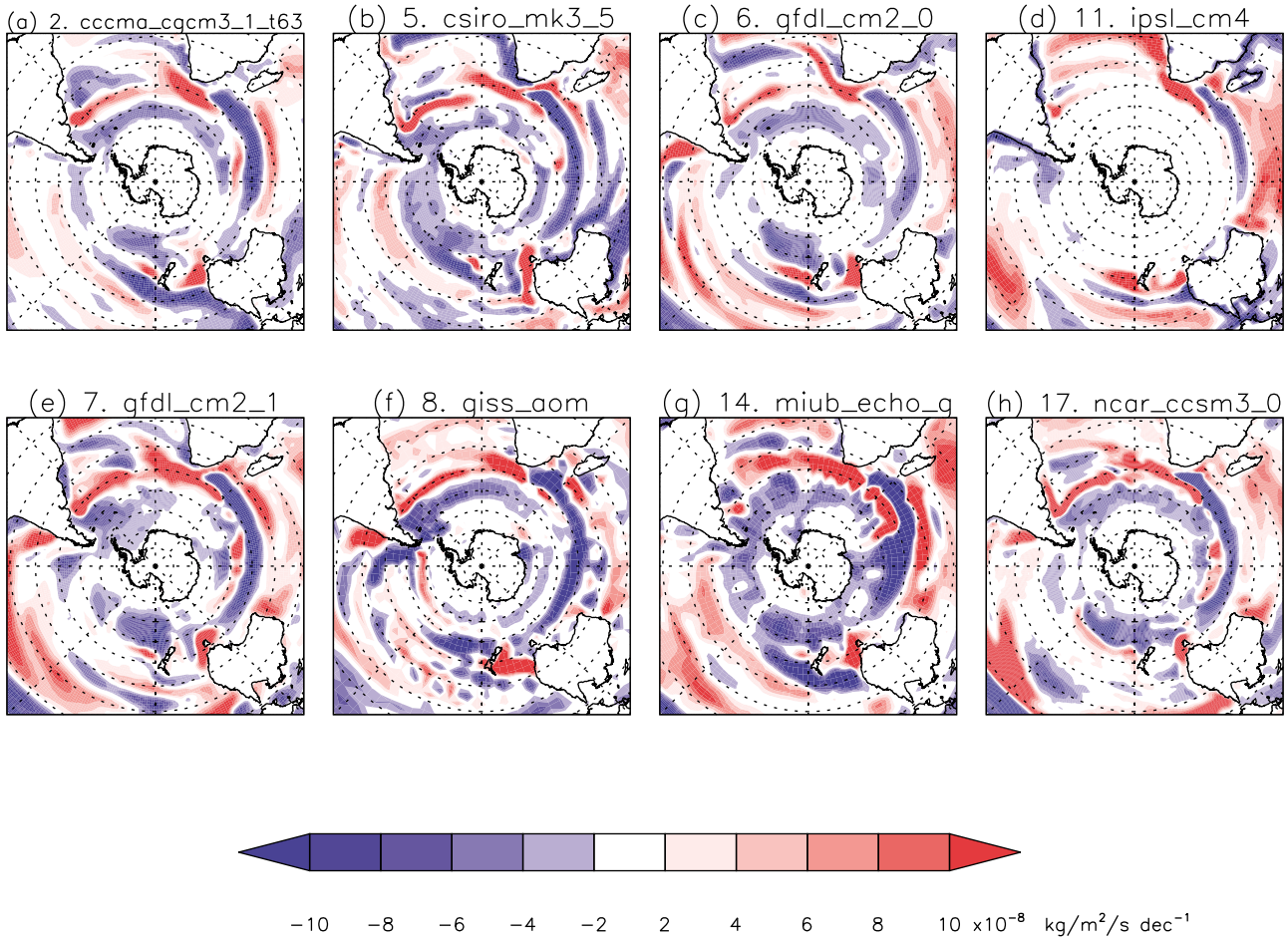

Figure 5. Linear trends in density flux (positive makes surface seawater denser) over the 21st century for the eight selected models.

ocean and increased P-E at higher latitudes (not shown). However, there are complex patterns at lower latitudes, characterized by bands of positive trends being mixed with bands of negative trends. The inconsistent spatial structure and magnitude of the density flux patterns suggest discrepancies across the models in capturing heat and freshwater fluxes.

5. Links Between ACC Trends and Trends in Momentum and Buoyancy Forcing

5.1. Links Between ACC Trends and the SAM Trends

[20] Figure 6 shows the ACC trends from Figure 1 plotted against the trends in SAM index shown in Figure 2. The best linear fit (black line) indicates that for a larger SAM index trend, there is a larger ACC trend, with the correlation coefficient of 0.41 ($p = 0.08$; p is the estimated probability of erroneously rejecting the null hypothesis), suggesting that the models with increased ACC transport generally show a larger increase in westerlies than those with decreased ACC transport. However, the scatter is large. For models 4, 5, 8, 10, 17, and 19, the SAM index trends are almost the same, but the ACC trends in these models are considerably different. This is also the case for models 2, 3, 6, 7, 12, and 16. Model 14 has the largest SAM index trend, but the ACC trend is negative. This suggests that other factors are also important in controlling the ACC transport changes.

5.2. Links Between ACC Trends and Trends in Wind Stress Curl

[21] To examine the relationship between the ACC trends and the trends in wind stress curl, we first find the domains of large-scale eastward flows, i.e., the domain between the subtropical gyre axes and the subpolar gyre axes. (As illustrated in Figure 9, the subtropical gyre axes are defined as the latitudes of maximum barotropic stream function, which is obtained by integrating the vertically integrated zonal transport from the coast of Antarctica to lower latitudes; similarly, the subpolar gyre axes are defined as the latitudes of minimum barotropic stream function. The domain is then divided evenly into southern and northern halves, with the separation between these occurring midway between the gyre axes. Another division, e.g., dividing the domain into southern and northern halves with the same total transport, does not qualitatively change the relationship shown in this and other relevant figures.) We then calculate the means of wind stress curl and density flux over the southern halves and the northern halves of the domains.

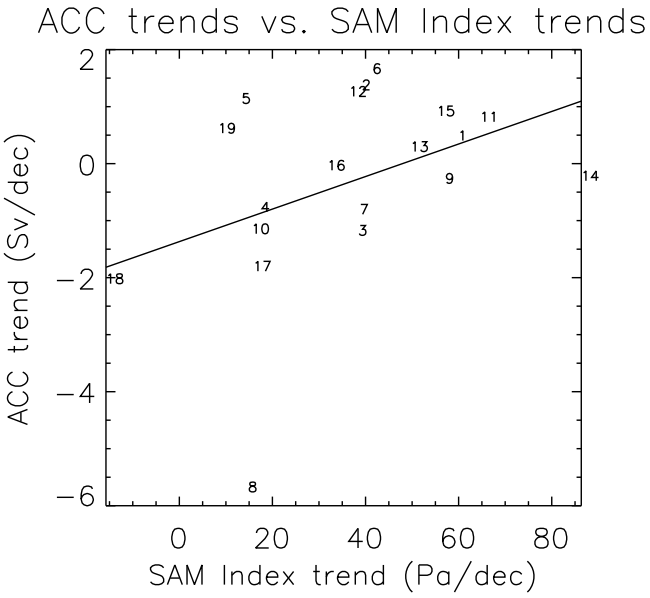

Figure 6. ACC trends against SAM index trends over the 21st century. The black line is the best linear fit.

The downward Ekman pumping (positive wind stress curl) in the northern halves and upward Ekman pumping (negative wind stress curl) in the southern halves are key processes in the set up of the isopycnal structures. We thus separately plot the trends in ACC transport against the trends in wind stress curl averaged over the southern halves (Figure 7a) and those averaged over the northern halves (Figure 7b).

[22] It is found that the averaged trends in wind stress curl shown in Figure 7 are generally consistent with SAM index trends in Figure 2, particularly for the northern half of the domain, i.e., a larger SAM trend corresponds to a larger trend in wind stress curl (compare also Figures 6 and 7). Comparing Figure 7b with Figure 7a, we find a much stronger link between the averaged trends in wind stress curl over the northern halves and the trends in the ACC transport, i.e., a larger downward Ekman pumping in the northern half of ACC domains corresponds to a larger increase in the ACC transport. This is plausible since, due to the stronger stratification there, the role of Ekman pumping is more effective in changing isopycnal structures (see also section 6.2). This stronger link is corroborated by the much larger correlation coefficients, which are 0.46 ($p = 0.05$) in Figure 7b but −0.02 ($p = 0.94$) in Figure 7a. In addition, a number of observational studies have shown the changes in dynamic height gradient across the ACC are dominated by changes at its northern edge (e.g., see the analysis of data from six occupations of a hydrographic section near 140E between October 1991 and September 1996 by *Rintoul and Sokolov* [2001]).

5.3. Links Between ACC Trends and Trends in Density Flux

[23] The plot of ACC trends against density flux trends in the southern parts of their domains (Figure 8a) (correlation coefficient of −0.24 with $p = 0.37$) shows that the density flux trends are negative in all models, consistent with positive trends in net heat input and positive trends in P-E there (not shown). This clearly indicates that in the southern halves the changes of buoyancy forcing tend to make the ocean surface lighter. However, there are no consistent changes for the northern halves, as shown in Figure 8b, with correlation coefficient between ACC trends and density flux trends of 0.24 ($p = 0.37$). The plot of the ACC trends against the south–north contrasts (averaged density fluxes over southern halves minus those over northern halves) of the density flux trend (correlation coefficient of −0.36 with $p = 0.16$) (Figure 8c) shows that the contrasts are almost all negative. This sign of buoyancy forcing change tends to reduce the meridional density gradient in the upper layer, opposite to the effect of increased Ekman pumping on the isopycnal structure, and hence tends to reduce the ACC transport. These are two competing processes that change the ACC transport, but the slope of the best linear fit

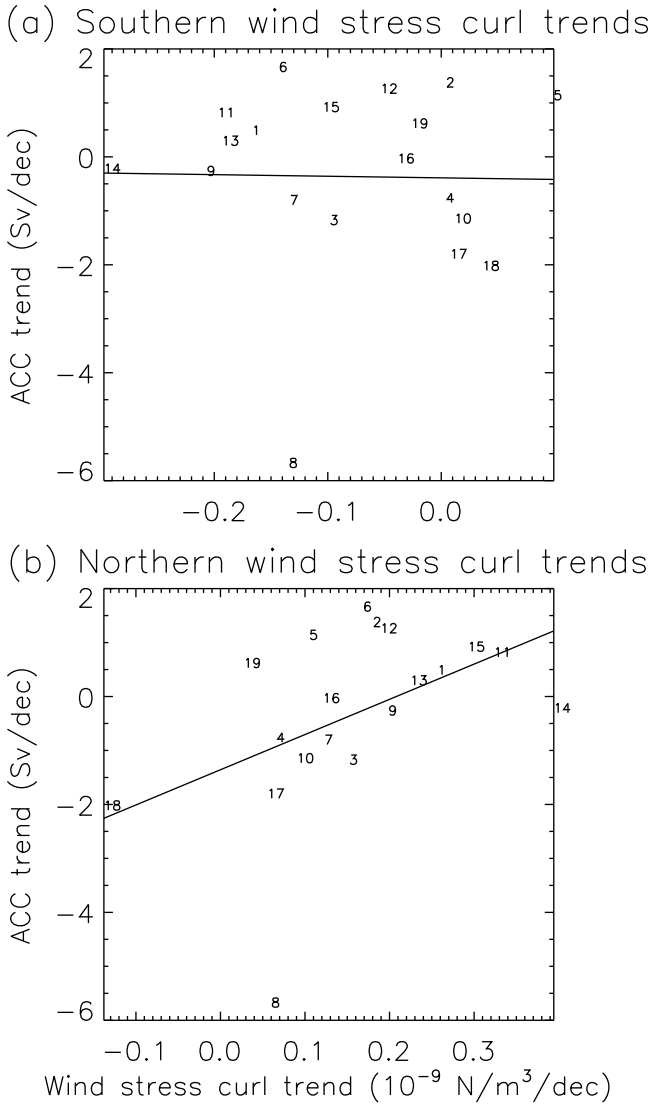

Figure 7. ACC trends against the trends in wind stress curl (a) averaged over the southern halves of the ACC eastward flow domains and (b) averaged over the northern halves of the domains.

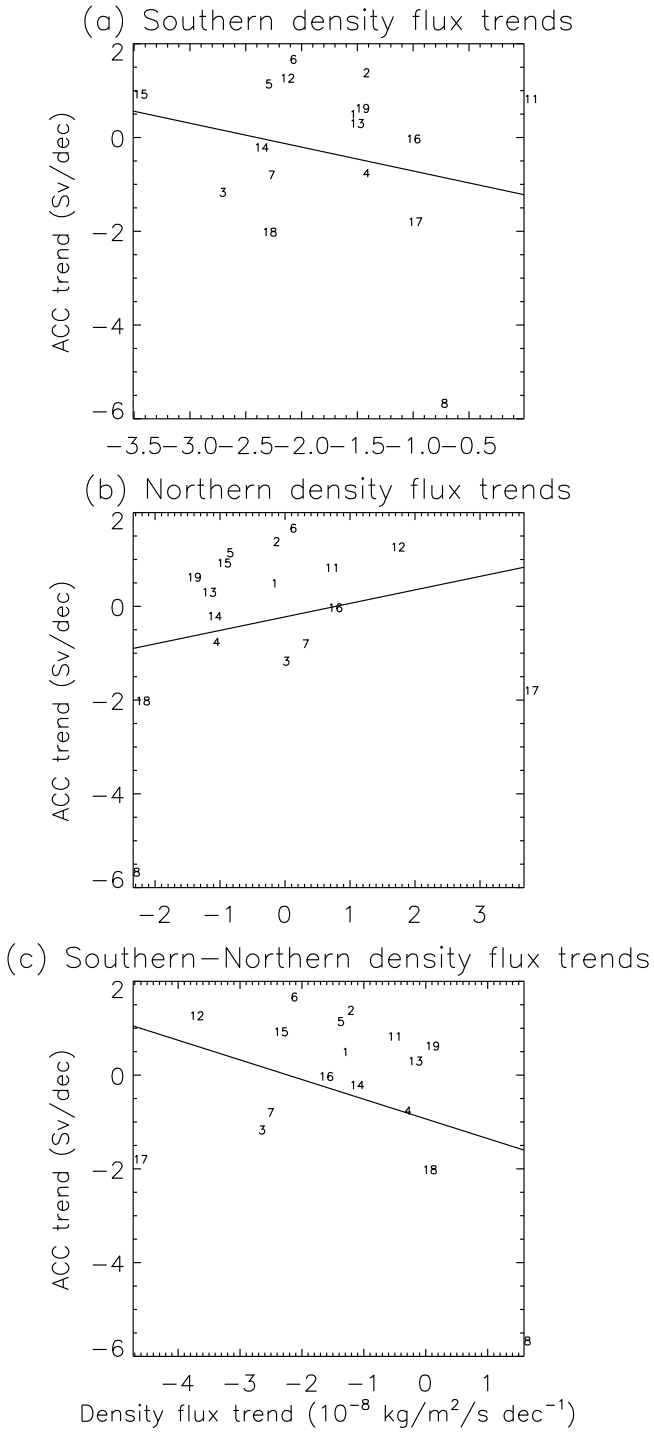

Figure 8. ACC trends against the density flux trends (a) averaged over the southern halves of the ACC domains, (b) averaged over the northern halves of the ACC domains, and (c) density flux trends averaged over the southern halves of the ACC domains minus those averaged over the northern halves of the ACC domains.

suggests that the wind effects are generally larger on the ACC transport changes across these models.

6. What Causes the Deceleration of the ACC Under Increased Wind Forcing?

6.1. Horizontal Structures of Zonal Transport Changes

[24] Figure 9 shows the horizontal structures of the trends in zonal transports for the 8 selected models with 4 models having significant positive trends in the ACC transport through Drake Passage (Figures 9a–9d) and the other 4 models having significant negative trends (Figures 9e–9h). The dashed green lines mark the northern and southern boundaries of the large scale eastward flows (defined as the latitudes of maximum and minimum barotropic stream function), and the dashed black lines mark the latitudes of maximum zonal transport, derived from the averaged zonal current over the first decade of the 21st century. Figures 9a–9d along with Figure 9e and Figure 9g show broad bands of obvious increases in the zonal transport, and clearly increased transports through Drake Passage in Figures 9a–9d, as responses to the increases of the westerlies (Figure 9g shows results from model 14, which has the largest increases of westerly winds and a small negative trend in ACC transport). Generally, the bands of increased zonal transports lie to the south of the maximum zonal transport, reflecting the poleward shifts of the peak ACC. *Fyfe and Saenko* [2006] showed that both the latitude of the peak ACC and the maximum strengths increased in 12 selected models. (Our streamwise averaged zonal means of the transport changes also show increased maximum ACC transports for these models, except for models 8 and 17.) In contrast, in models 8 and 17 (Figure 9f and 9h), there are patchy increases of the zonal transport, mixed with relatively broad areas of decreased zonal transport. The maximum strengths in these models become significantly decreased at various locations. Note that these models have small increases of the westerlies, as shown in Figure 2. Also, the models with decreased ACC generally do not have well defined maximum transport belts in the SO.

[25] A noteworthy common feature of the transport changes in all these models is that the northern boundaries of the eastward flow shift poleward considerably. Also, there are very broad bands of decreased transports to the south of the northern ACC boundaries. The poleward shift of the subtropical westward flows was also reported by *Cai et al.* [2005] and *Saenko et al.* [2005], and *Sen Gupta et al.* [2009] also noticed such shifts in IPCC AR4 models. In contrast, there are no consistent shifts of the southern ACC boundaries among these models. Through comparing Figures 9a–9d with Figures 9e–9h, however, we see another noteworthy feature. In Figures 9a–9d, generally, there are no negative trends at and to the north of the southern ACC boundaries (except for Figure 9d in the Ross Sea). This clearly indicates that there are generally no equatorward expansions of the westward flows in the subpolar gyres, which appears to run counter to the finding by *Beckmann et al.* [1999] that the increase of cyclonic wind stress forcing in the subpolar region can intensify the subpolar gyres.

Figure 9. Trends in vertically integrated zonal transport for the eight selected models. The dashed green lines mark the northern and southern boundaries of the large-scale eastward flows (see text for definitions), and the dashed black lines mark the locations of maximum zonal transport, derived from the averaged zonal current over the first decade of the 21st century.

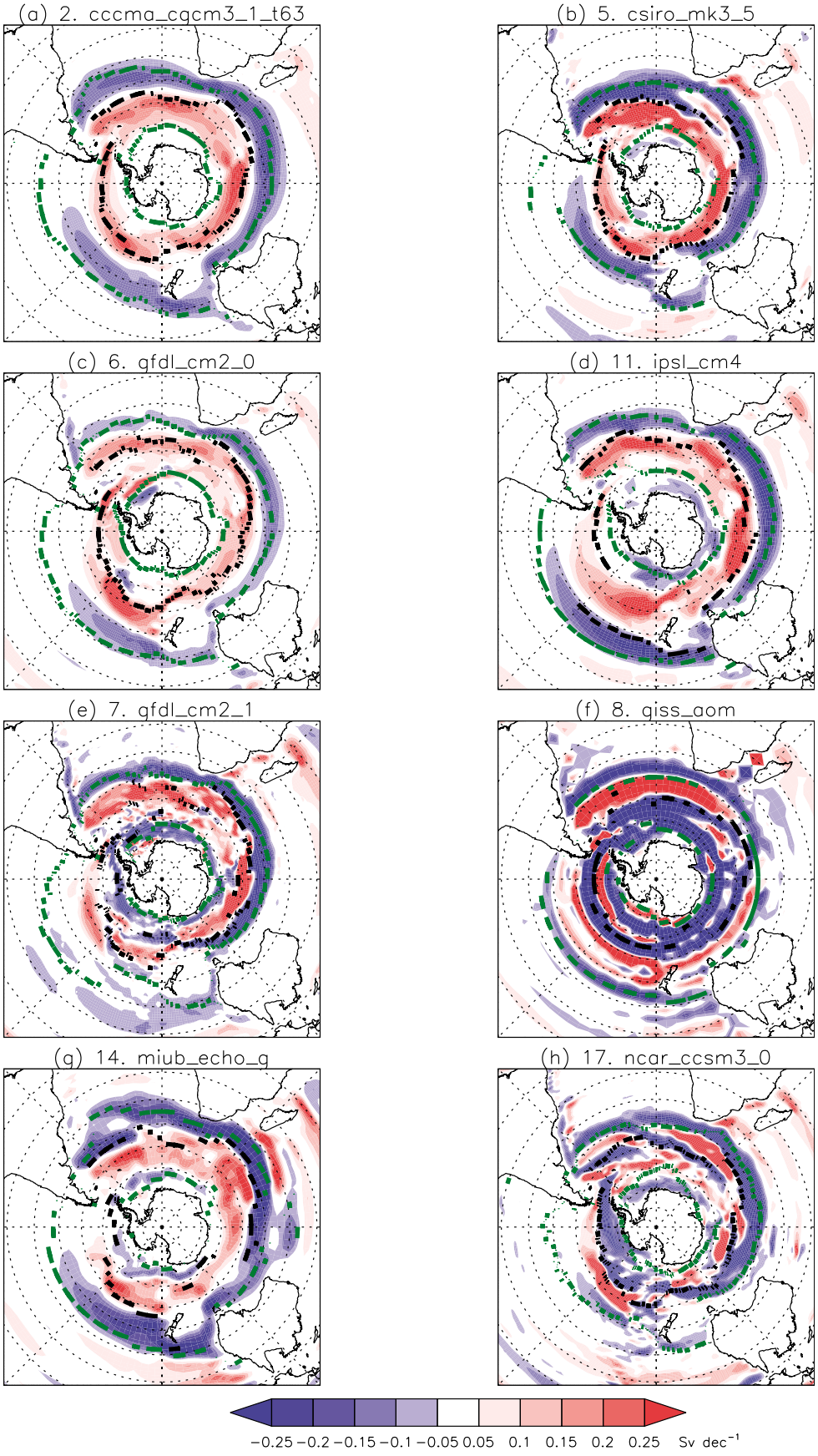
(a) 2. cccma_cgcm3_1_t63
(b) 5. csiro_mk3_5
(c) 6. gfdl_cm2_0
(d) 11. ipsl_cm4
(e) 7. gfdl_cm2_1
(f) 8. giss_aom
(g) 14. miub_echo_g
(h) 17. ncar_ccsm3_0
−0.25 −0.2 −0.15 −0.1 −0.05 0.05 0.1 0.15 0.2 0.25 Sv dec^{-1}

Figure 9

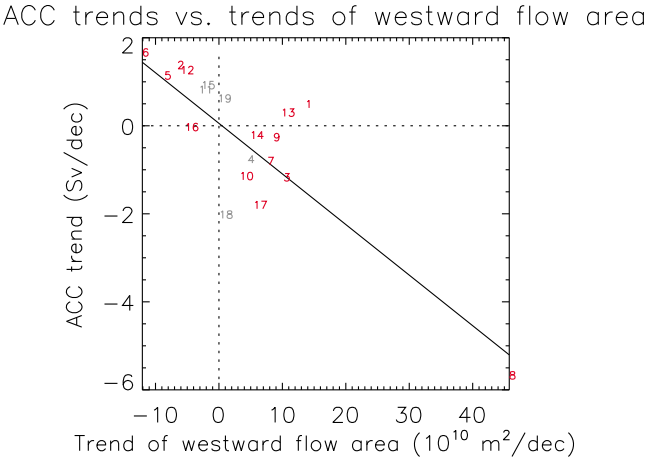

Figure 10. ACC trends against the trends in westward flow area in the subpolar region. The trends in grey for the westward flow areas are not statistically significant at the 5% level.

In Figures 9e–9h, there are much more broad areas of decreased eastward (or increased westward) transports at and to the north of southern ACC boundaries, clearly indicating equatorward expansions of the westward flows in the subpolar gyres.

[26] To further illustrate the relationship between the ACC transport trends and the changes of the subpolar gyre sizes, we plot the ACC transport trends against the trends in the westward flow area of the subpolar gyres in Figure 10. Generally, for those models with decreased ACC transports, there are equatorward expansions of the subpolar westward flows, and similarly the increased ACC transports correspond to the poleward contracted subpolar westward flows (correlation coefficient of −0.84 with $p < 0.01$); the expansion is the largest for model 8, which has the largest decrease in the ACC transport. Although the exceptions (e.g. models 1 and 13) suggest that increased ACC transports do not necessarily correspond to poleward contractions of the subpolar westward flows, there are significant increases of the westward flow areas for all the models that have decreased ACC transports. Further (more controlled) studies are needed to investigate the causes and effects in the dynamical coupling between the ACC and the subpolar gyres.

[27] Overall, we find that the decreases in the ACC transports, where found in the models, are associated with the reduced eastward transports on the northern and southern flanks (around the northern and southern boundaries) of the ACC. If the reduced transports around the northern and southern boundaries are not compensated by the increased transports in the interior region, the total transports will decrease. Note that the changes of transports on the northern flanks are generally much larger than those on the southern flanks, as shown in Figure 9. Since the currents are mainly in geostrophic balance, the interior transport increases are dependent on the steepening of isopycnal surfaces that can be affected by external forcing, such as wind and buoyancy forcing, and by internal oceanic processes, such as stratification and (parameterized) eddy-induced transport.

6.2. Processes That Affect the Stratification

[28] One of the processes that changes the isopycnal structure is the change in downward Ekman pumping in the subtropics/midlatitudes. As illustrated in Figure 4, the maximum wind stress curl in the subtropics/midlatitudes becomes larger and shifts poleward, and Figure 7 suggests that the ACC trends are more correlated with the changes in wind stress curl at lower latitudes. The Ekman pumping effect on the isopycnal structure is determined by the product of wind stress curl and density stratification [e.g., *Gill*, 1982]. For models with almost the same wind stress curl changes, the variations in density stratifications are responsible for the different Ekman pumping effects. For example, for models 4, 5, 8, 10, 17, and 19, the zonal wind stress changes are almost the same, but models 4, 8, 10, and 17 have reduced ACC transports. Figure 11 shows that these four models have weaker stratifications averaged over 45°S–35°S than models 5 and 19; in particular, the stratification is the weakest in model 8, which has the largest decrease of the ACC transport. In a weakly stratified model, the wind-induced downward displacement of only slightly lighter waters does not affect much the large-scale meridional density gradient that balances the ACC. Thus the effect of the strengthened Ekman pumping is limited. Conversely, in strongly stratified models (5 and 19) a similar vertical displacement matters much more. This increases the meridional density gradient, and a larger ACC transport can be balanced. (Note that model 17 has stronger stratification than models 4 and 10, but a larger decrease of the ACC transport as shown in Figures 1 and 6; this is discussed below.) These results indicate that stratification at lower latitudes has a very important effect on the response of the ACC transport to the strengthening of the westerlies in these models.

[29] Eddy-induced mass transport is believed to be a key process in both the dynamical and thermodynamical balances in the SO [*Marshall and Radko*, 2003]. The strengthening of the westerlies acts to increase the isopycnal slopes, while the

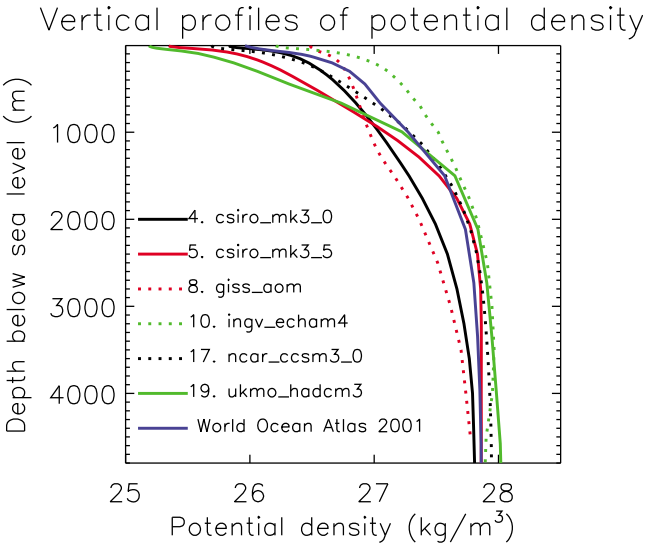

Figure 11. Vertical profiles of zonally averaged potential density anomaly over 45°S–35°S and over the first decade of the 21st century for models 4 (solid black), 5 (solid red), 8 (dashed red), 10 (dashed green), 17 (dashed black), and 19 (solid green). Note that the profiles in colors have weaker stratifications, corresponding to negative ACC transport trends for models 4, 8, 10, and 17. The profile in blue is derived from World Ocean Atlas 2001 [*Conkright et al.*, 2002].

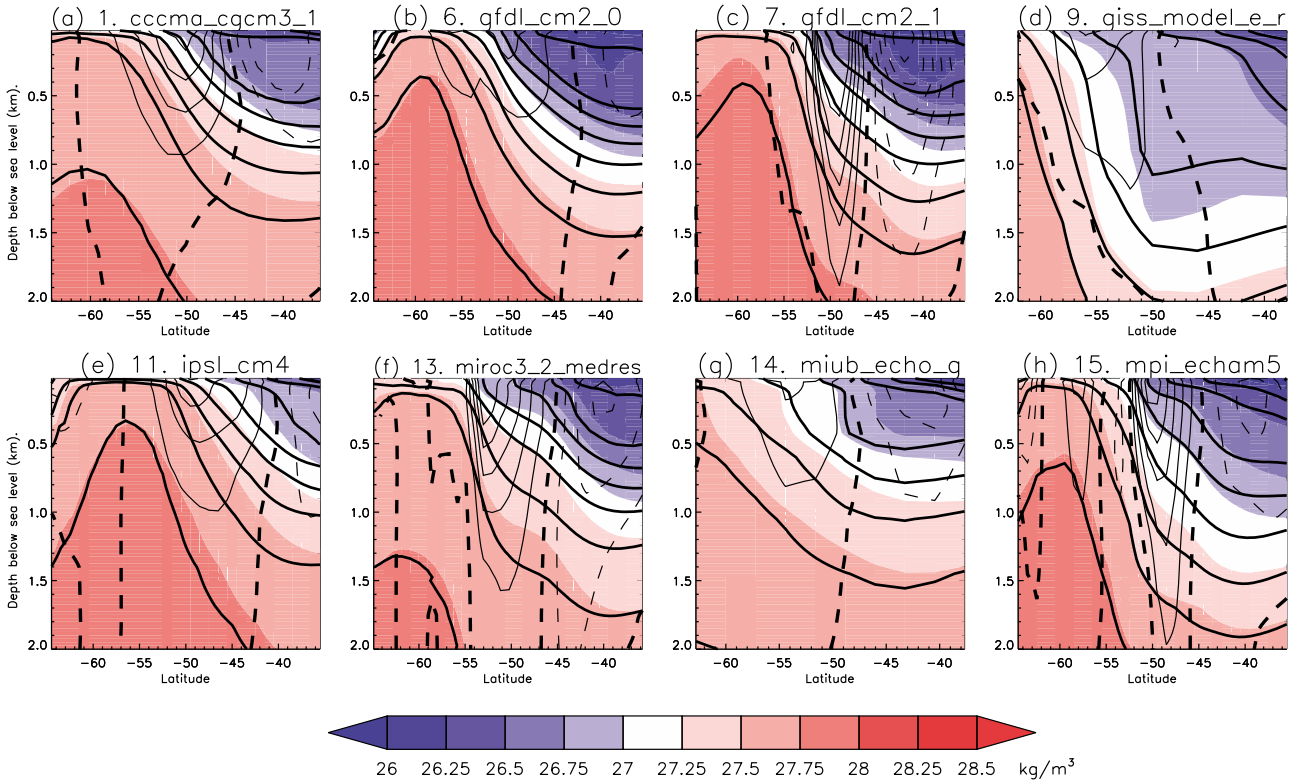

Figure 12. Latitude-depth cross sections at 90°E of potential density anomaly averaged over the first decade (color shading) and averaged over the last decade (thick solid black lines) of the 21st century. The trends in zonal velocity are also shown (contour interval is 10^{-3} m s^{-1} $decade^{-1}$, thin sold lines are for positive values, thin dashed lines are for negative values, and the zero lines are highlighted in bold dashed lines).

associated eddy response tends to reduce them. The eddy processes are not resolved and have to be parameterized in coarse-resolution models. Although the eddy parameterizations have various forms in CMIP3 models (see Table 1), in most of them the eddy-induced transports are either a linear or a roughly quadratic function of the slopes, depending on the choice of the coefficient in the parameterization (constant or diagnosed from the stratification). In either case, the increases in isopycnal slopes result in increased eddy-induced mass transports that tend to flatten the isopycnal surfaces. Experiments with an eddy-permitting ocean model [*Hallberg and Gnanadesikan*, 2006] suggest that the sensitivity of the SO circulation to wind stress changes is greatly reduced in the presence of eddies. This result has recently been corroborated with a global coupled climate model that contains an eddy-permitting ocean [*Farneti and Delworth*, 2010]. While the parameterizations for eddy transports used in the AR4 models are known to be imperfect, they will nonetheless act to reduce ACC transports relative to the level they would otherwise reach.

[30] Figure 12 illustrates the changes over the 21st century in isopycnal surfaces in eight selected models with relatively large increases in westerlies. Associated with large increases in eastward flow, we find a steepening of isopycnal surfaces in these eight models. The steepening can consequently lead to enhanced eddy-induced transports, which have the effect of flattening isopycnal surfaces and retarding the increase in ACC transport. For a model with large isopycnal thickness diffusion or a large smoothing effect on the isopycnal structure induced by parameterized eddy transport, a large increase in isopycnal slope cannot be maintained even under a very large increase of the westerlies. This process, when acting in combination with a narrowing of the ACC, can lead to a reduction in the transport. A quantified intercomparison study of the diffusions of the isopycnal thickness by parameterized eddy transports in these models would, however, require more information on parameterized eddy velocity than is provided by each modeling group. It is thus very important for the next model comparison projects to provide such data to quantify the parameterized eddy transports in coupled climate models.

[31] We have shown in Figures 5 and 8 that increased westerlies have associated changes in buoyancy forcing that tend to make the surface water denser at lower latitudes and lighter at higher latitudes. Thus, changes in buoyancy forcing also tend to reduce the meridional density gradient in the upper layer. For example, in Figure 11, model 17 has the largest stratification (see the green dashed line) among those models with decreased ACC transports, and the decrease of the ACC transport is large relative to those in models 4 and 10. In models with small increases of the westerlies, the effects of Ekman pumping on the meridional density gradient are relatively small. Thus, the changes of parameterized eddy transports should be reasonably small. It is possible that the

large south–north contrast of density flux change, as seen in Figure 8, makes a considerable contribution to the slowdown of the ACC in model 17. This large south–north contrast of density flux change tends to reduce the meridional density gradient in the upper layer, and to weaken the ACC.

6.3. Discussion

[32] *Russell et al.* [2006] proposed that weaker, shallower, and less dense (fresher or warmer) North Atlantic Deep Water (NADW) in the SO can lead to lower density on the southern side of the ACC and hence a weaker ACC transport. In a warming climate, these IPCC AR4 models have generally weakened NADW formation, and model 8 has the largest such weakening [see *IPCC*, 2007, chapter 10]. According to *Russell et al.* [2006], the weakening of Atlantic MOC in these models have the potential to decelerate the ACC. On the other hand, however, the weakening of the Atlantic MOC can lead to the deepening of the thermocline on the northern side of the ACC and hence can lead to an increase in the ACC transport [*Fučkar and Vallis*, 2007]. Our analysis indicates that relatively large simulated density changes in the SO are confined to the upper layers (see Figure 12). Considering this, and that most models with increased ACC transports shown in Figure 1 have the weakening of the NADW formation [see *IPCC*, 2007, chapter 10], we suggest that the weakening of Atlantic MOC has a minor contribution to decreasing the ACC transport.

[33] We have identified several large-scale processes that can effectively change isopycnal structure and hence the ACC transport. Associated with the strengthening of the westerlies, there is increased downward Ekman pumping on the northern side and increased upward Ekman pumping on the southern side of the ACC. This process acts to increase the upper layer meridional density gradient and hence to increase the eastward transport. However, the accompanying narrowing of the ACC, mainly caused by large poleward shifts of the subtropical gyres and to a lesser extent by the equatorward expansions of the subpolar gyres, can reduce the total transport when combined with other processes, such as weak Ekman pumping effects induced by weak stratifications, enhanced eddy-induced transports, and associated buoyancy forcing.

[34] It is a common feature that the ACCs become narrower under increased westerlies in these models. To the extent that this occurs also in the real ocean (as opposed to e.g. the fronts becoming closer together with unchanged isopycnal slopes within them), it has strong implications for the status of eddies in the ACC region. The fact that the observed decadal scale ACC transport remained relatively unchanged during the past several decades [e.g., *Böning et al.*, 2008] indicates that several processes, including eddies [e.g., *Meredith and Hogg*, 2006], play an important role in constraining the ACC transport. The narrowing of the ACC system would reduce the ACC transport on the northern flank (and possibly also on the southern flank) of the ACC. If the ACC is eddy saturated on decadal timescales (i.e., an increase in wind forcing leading only to an increase in eddy transports, without an increase in isopycnal slopes), the increased Ekman pumping effects can only increase the eddy kinetic energy, rather than the gradient of potential energy or isopycnal slopes across the narrower ACC. This would lead to an unchanged zonal transport across a narrower section. Therefore, the total mean ACC transport would decrease, which is, however, not observed by *Böning et al.* [2008].

[35] A process that is difficult to analyze, and which has not been investigated here, is the interaction between bottom topography and circulation. The current changes induced by atmospheric forcing changes could lead to different interactions between these. The examinations of changes in bottom pressure torques [*Wells and de Cuevas*, 1995; *Hughes and de Cuevas*, 2001] may offer some understanding of the roles of bottom topography in the responses of the ACC to atmospheric forcing changes. However, for most models the data available at the PCMDI database do not permit calculation of this term with sufficient accuracy. The reasons are i) that most modeling groups interpolated the data horizontally and/or vertically (which was a requirement) and ii) the gradient calculations of bottom pressure and bottom topography cannot be repeated exactly as in each individual model.

7. Concluding Remarks

[36] There are considerable discrepancies in the responses of the ACC to increased westerlies over the 21st century in IPCC AR4 models. Under increased wind forcing, some models even predict reduced ACC transports over the 21st century. We have examined the major large-scale processes that are responsible for the diverse responses of the ACC transport to the increases of westerlies.

[37] Associated with eastward wind stress increases, the changes in buoyancy forcing (density flux) generally tend to reduce the upper layer meridional density gradients. The analysis of isopycnal structure changes indicates that there are increased parameterized eddy-induced transports in response to the increases of westerlies. The enhanced eddy activities tend to flatten the isopycnal surfaces, hence contributing to reducing the ACC transports.

[38] There are considerable poleward shifts of the subtropical gyres, caused by the poleward shifts of the westerly axes. In the subpolar region, there is generally increased cyclonic wind forcing that tends to strengthen the subpolar cyclonic circulation. In the models with reduced ACC transports, there is a significant equatorward expansion of the subpolar westward flow. These processes, mainly the poleward shifts of the subtropical gyres, lead to the narrowing of the ACC. The narrowing of the ACC appears to act to limit the increases in the total ACC transports in these IPCC AR4 models, when combining with associated buoyancy forcing changes and enhanced parameterized eddy-induced transports.

[39] The strengthening of the westerlies and associated enhanced Ekman pumping effects are primarily responsible for increasing the isopycnal slopes and hence tend to increase the ACC transport. Our analysis has shown that the changes in the wind stress curl at lower latitudes are more dominant in changing the ACC transport, because the ocean density stratification is much larger there than at higher latitudes, and hence the Ekman pumping effects on isopycnal structures are much larger. For the same reason, in some models with almost the same increase in wind forcing, those models with weak stratifications at lower latitudes have reduced ACC transports, partially attributable to the weak Ekman pumping effects.

[40] We have seen that large-scale processes are important in controlling the evolution of the ACC transport under

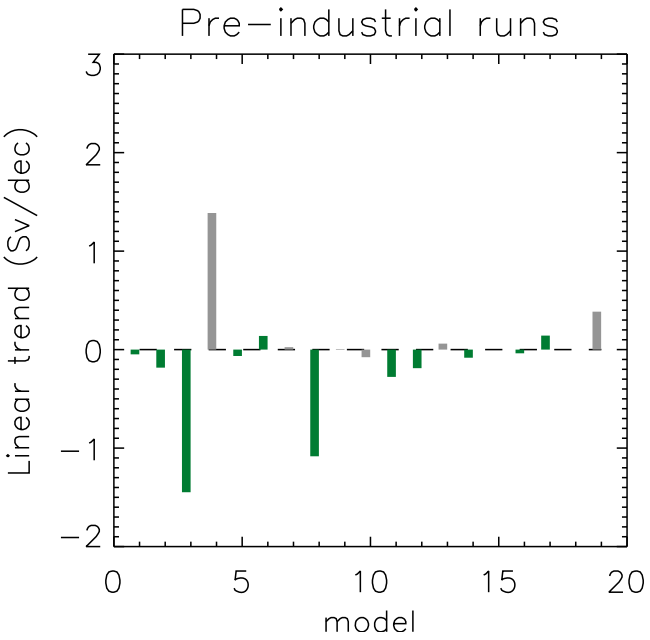

Figure A1. Linear trends in the total ACC transports through the Drake Passage in preindustrial runs. The trends in grey are not statistically significant at the 5% level.

climatic change. The examination of these processes offers some important understanding of the diverse response of the ACC transport under increased wind forcing in these models, and of the observed relative insensitivity of the ACC transport to large changes in wind forcing on decadal timescales during the past several decades. Future, more complete, understanding of the ACC responses to climate changes requires more realistic representations of both large-scale and small-scale (e.g., eddy induced) processes in global coupled climate models. At the same time, given the complex and sensitive nature of ACC transport change to different large-scale forcings seen here, it is perhaps the case that the future of the real ACC transport remains very uncertain, even to the extent that a deceleration cannot be ruled out. Given the large-scale connectivity facilitated by the ACC, this has potential implications for regional and global climate.

Appendix A: Model Drifts in Preindustrial and Commit Runs

[41] In this appendix, we analyze the model drifts in the ACC transport in preindustrial and commit runs, and we demonstrate that the changes in the ACC transport in sresa1b runs are caused by climate changes, rather than by model drifts, in most models.

[42] The corresponding trends in ACC transport through Drake Passage for the preindustrial runs are generally very small (Figure A1). However, models 3, 4 and 8 have very large trends, indicating that these models have large drifts in their control runs. (Note that the large positive trend in model 4 is not statistically significant since this model has large multidecadal variability in the control run.) The very small trends for most of the models indicate that the ACC is generally very stable in their control runs.

[43] The comparison between Figures 1 and A1 indicates that the significant negative trends for models 7, 8, 10, 14, 17 and 18 in Figure 1 are not caused by the model drifts in the control runs. We note that there is a relatively large negative trend (−1.1 Sv decade^{-1}) for model 8 during the preindustrial run, but the negative trend in its sresa1b run (−5.76 Sv decade^{-1}) is much larger.

[44] To further analyze the drifts in the ACC transport, we first calculated the trends in the ACC transport through Drake Passage in commit runs, and then we present the trends in the vertically integrated zonal transport in both commit and sresa1b runs for 14 models. (Note that only 14 models have their corresponding commit runs.) The commit runs are parallel runs to sresa1b runs over the 21st century, but with fixed greenhouse forcing at the end of the 20th century.

[45] The linear trends in the ACC transport through Drake Passage and trends in SAM index for both sresa1b and commit runs are shown in Table A1. To facilitate the comparisons here and below, we divide these 14 models into three groups. For the first group, in the commit runs, models 3, 6, 9, and 19 have very close changes in the ACC transport through Drake Passage to those in their sresa1b runs. For the second group, the trends in the sresa1b runs are much larger

Table A1. The Trends in the ACC Transport Through Drake Passage and Trends in SAM Index for Both sresa1b Runs and Commit Runs of 14 Models[a]

Model Number	Model Name	ACC (sresa1b)	ACC (commit)	SAM (sresa1b)	SAM (commit)
1	cccma_cgcm3_1	0.40(0.00)	−0.34(0.00)	59.90(0.00)	−4.56(59.93)
3	cnrm_cm3_0	−1.26(0.00)	−1.11(0.00)	38.47(0.00)	−2.46(77.97)
4	csiro_mk3_0	−0.85(23.45)	−0.19(71.90)	17.58(0.24)	−5.84(37.14)
5	csiro_mk3_5	1.06(0.00)	0.53(0.00)	13.45(0.97)	−2.27(68.94)
6	gfdl_cm2_0	1.58(0.00)	1.43(0.00)	41.55(0.00)	−27.88(0.65)
7	gfdl_cm2_1	−0.89(3.79)	−0.15(50.19)	38.78(0.00)	8.73(20.64)
9	giss_model_e_r	−0.35(2.69)	−0.33(6.11)	57.17(0.00)	−7.15(32.35)
11	ipsl_cm4	0.73(0.00)	0.28(0.01)	64.60(1.68)	10.58(60.81)
13	miroc3_2_medres	0.21(39.25)	−0.35(29.76)	49.65(0.02)	−2.45(81.39)
14	miub_echo_g	−0.30(0.01)	0.10(38.64)	86.34(0.00)	10.75(24.32)
16	mri_cgcm2_3_2a	−0.12(31.97)	−0.37(0.00)	31.80(0.47)	−6.80(39.62)
17	ncar_ccsm3_0	−1.89(0.00)	−0.86(0.01)	15.88(0.29)	5.42(38.09)
18	ncar_pcm1	−2.10(0.05)	−1.54(0.07)	−15.76(11.63)	−0.65(94.47)
19	ukmo_hadcm3	0.53(0.01)	0.74(65.70)	8.32(34.13)	4.46(45.69)

[a]The units for trends in the ACC transport through Drake Passage are Sv decade^{-1}, and the units for trends in SAM index are Pa decade^{-1} for both sresa1b runs and commit runs of 14 models. The significance levels are given in parentheses (in percentage).

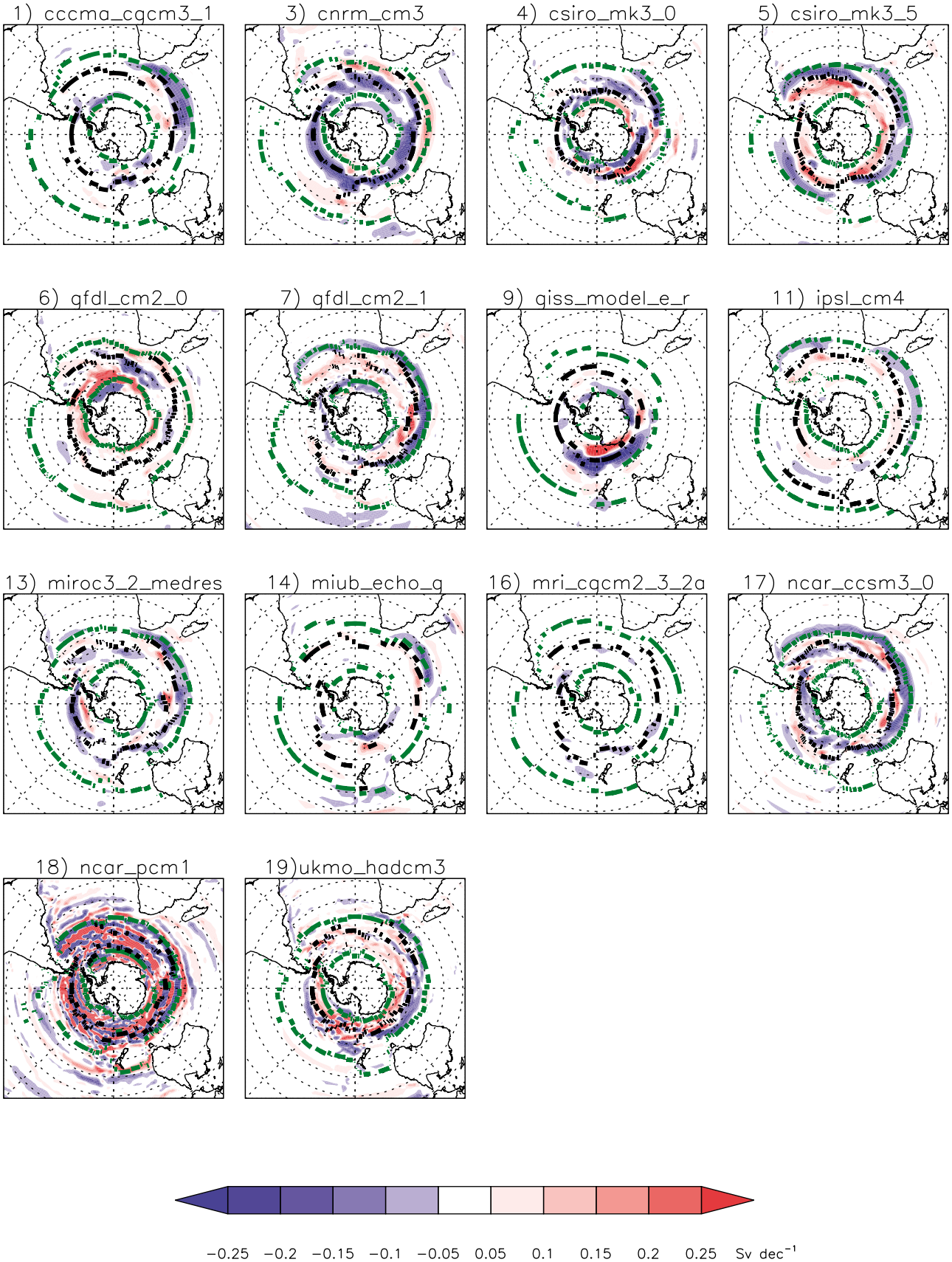

Figure A2. Similar to Figure 9 but for the commit runs of the 14 models listed in Table A1.

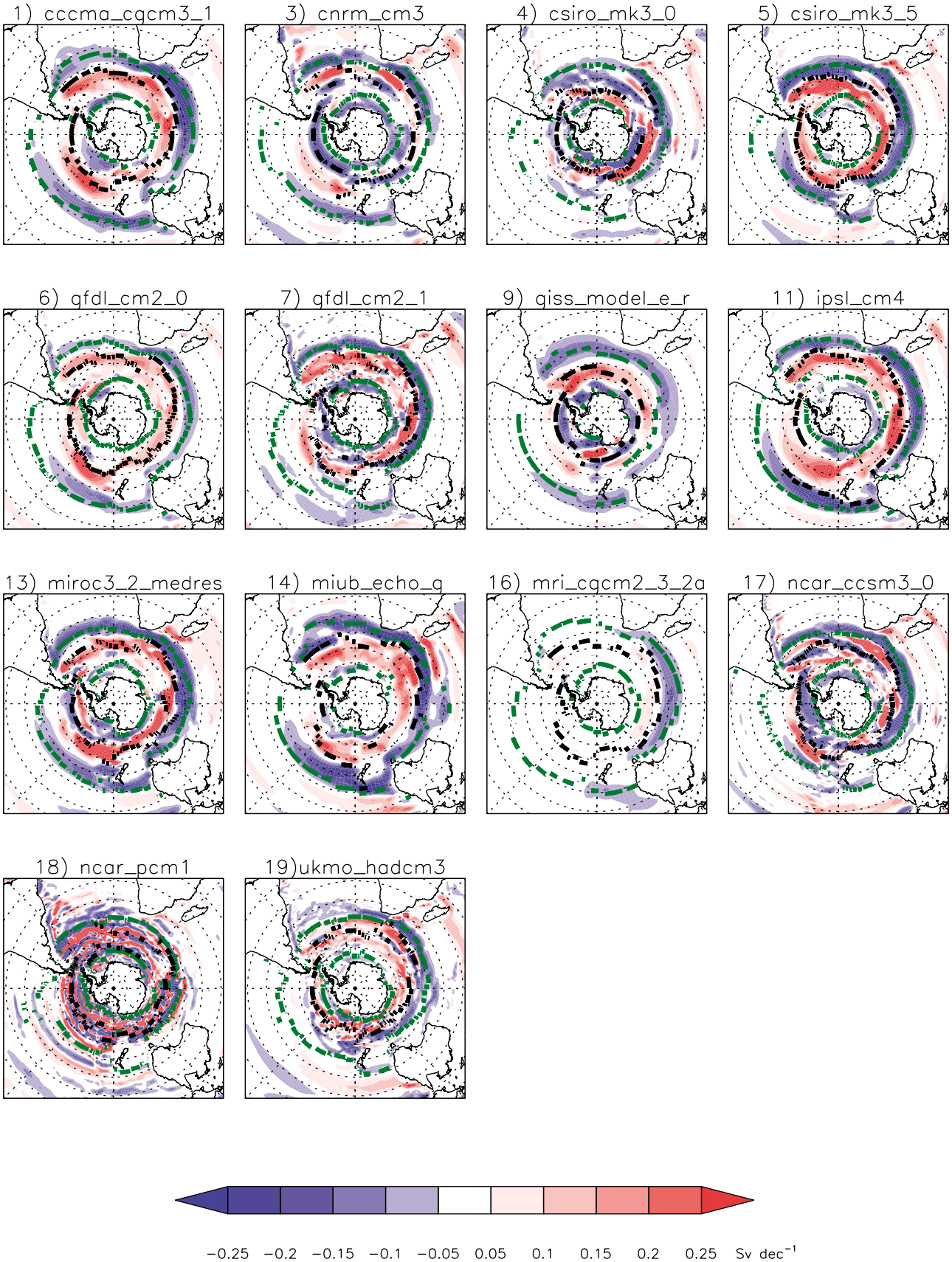

Figure A3. Similar to Figure 9 but for 14 models listed in Table A1.

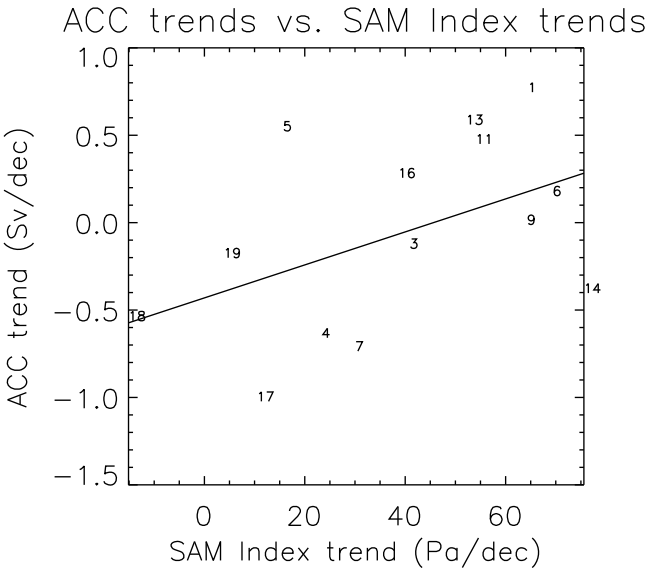

Figure A4. Similar to Figure 6 but the trends are adjusted by subtracting the trends in commit runs from those in sresa1b runs.

than those in the commit runs, although the trends for models 5, 17 and 18 are not small in the commit runs. For the third group, the trends for the rest models are very small in the commit runs, or even of opposite signs to those in the sresa1b runs. It is worth pointing out that those models with significant decreasing ACC transport in their sresa1b runs (models 4, 7, and 14) have either very small negative trends (models 4 and 7) or even a positive trend (model 14) in their commit runs, indicating the decreasing ACC transports in these three models are not caused by the model drifts. Table A1 also shows that the changes in SAM index are very small and not statistically significant in the commit runs, except for model 6.

[46] The crucial analysis to demonstrate that the changes in the ACC transport shown in Figure 9 result from responses to climate changes is to compare these changes in the commit runs with those in the sresa1b runs. Similar to Figure 9, Figure A2 shows the trends in the vertically integrated zonal transport for the commit runs in 14 models listed in Table A1, and Figure A3 shows the results for the sresa1b runs. For the first group, although models 3, 6 and 9 have almost the same changes in the ACC transport through Drake Passage in the commit runs as those in the sresa1b runs, the patterns of the ACC transport changes are very different. In the sresa1b runs for models 3, 6 and 9, there are obvious and significant decreasing transports around the northern boundaries and increasing in the interior of the ACC region, clearly resulting from responses to the changes in wind forcing as analyzed in section 6.1, while these changes cannot be seen in their commit runs. For the second group, it can be easily seen that the changes are much larger in the sresa1b runs than in the commit runs in models 5 and 17. For the third group, we see very sharp contrasts between the commit runs and the sresa1b runs, with the changes in the commit runs being very small over very broad area. The contrasts are particularly clear in those models with large wind changes in the sresa1b runs, e.g., for models 11 (with increased ACC transport through Drake Passage) and 14 (with decreased transport through Drake Passage). These comparisons clearly demonstrate that the analyzed changes in the ACC transport are caused by climate changes in most models, rather than by the model drifts.

[47] Based on the above analysis, we refrained from replotting Figures 6–8 using adjusted trends (through subtracting the trends in commit runs from those in sresa1b runs). The above analysis indicates that the drifts in the commit runs may not remain linearly in the sresa1b runs or may not form the substantial parts in the trends in the sresa1b runs. For example, for models 3, 6 and 9 with the same trends in the commit runs and in the sresa1b runs, there are sharp contrasts in the spatial distributions of the changes in the vertically integrated zonal transport between the commit runs and the sresa1b runs, suggesting that the ACC transports through Drake Passage are changed by quite different processes. (It is out of the scope of this paper to investigate what causes the ACC changes in the commit runs.) Even under the assumption that all drifts can linearly remain in the sresa1b runs, in the figures with adjusted trends (e.g., Figure A4), we found that our results drawn from Figures 6–8 remain qualitatively unchanged.

[48] **Acknowledgments.** We acknowledge the modeling groups, the Program for Climate Model Diagnosis and Intercomparison (PCMDI), and the WCRP's Working Group on Coupled Modeling (WGCM) for their roles in making available the WCRP CMIP3 multimodel data set. T. Kuhlbrodt was supported by a Marie Curie IntraEuropean Fellowship within the 7th European Community Framework Programme.

References

Aoki, S. (2002), Coherent sea level response to the Antarctic Oscillation, *Geophys. Res. Lett.*, *29*(20), 1950, doi:10.1029/2002GL015733.

Beckmann, A., H. H. Hellmer, and R. Timmermann (1999), A numerical model of the Weddell Sea: Large-scale circulation and water mass distribution, *J. Geophys. Res.*, *104*, 23,375–23,391.

Bi, D., W. F. Budd, A. C. Hirst, and X. Wu (2002), Response of the Antarctic Circumpolar Current transport to global warming in a coupled model, *Geophys. Res. Lett.*, *29*(20), 2173, doi:10.1029/2002GL015919.

Böning, C. W., A. Dispert, M. Visbeck, S. R. Rintoul, and F. U. Schwarzkopf (2008), The response of the Antarctic Circumpolar Current to recent climate change, *Nat. Geosci.*, *1*, 864–869, doi:10.1038/ngeo362.

Cai, W., G. Shi, T. Cowan, D. Bi, and J. Ribbe (2005), The response of the Southern Annular Mode, the East Australian Current, and the southern midlatitude ocean circulation to global warming, *Geophys. Res. Lett.*, *32*, L23706, doi:10.1029/2005GL024701.

Conkright, M. E., R. A. Locarnini, H. E. Garcia, T. O'Brien, T. P. Boyer, C. Stephens, and J. I. Antonov (2002), *World Ocean Atlas* 2001*: Objective Analyses, Data Statistics, and Figures* [CD-ROM], *Intern. Rep. 17*, 17 pp., Natl. Oceanogr. Data Cent., Silver Spring, Md.

Cunningham, S. A., S. G. Alderson, B. A. King, and M. A. Brandon (2003), Transport and variability of the Antarctic Circumpolar Current in Drake Passage, *J. Geophys. Res.*, *108*(C5), 8084, doi:10.1029/2001JC001147.

Farneti, R., and T. L. Delworth (2010), The role of mesoscale eddies in the remote oceanic response to altered Southern Hemisphere winds, *J. Phys. Oceanogr.*, *40*, 2348–2354.

Fučkar, N. S., and G. K. Vallis (2007), Interhemispheric influence of surface buoyancy conditions on a circumpolar current, *Geophys. Res. Lett.*, *34*, L14605, doi:10.1029/2007GL030379.

Fyfe, J. C., and O. A. Saenko (2006), Simulated changes in the extratropical Southern Hemisphere winds and currents, *Geophys. Res. Lett.*, *33*, L06701, doi:10.1029/2005GL025332.

Gent, P. R., and J. C. McWilliams (1990), Isopycnal mixing in ocean circulation models, *J. Phys. Oceanogr.*, *20*, 150–155.

Gent, P. R., J. Willebrand, T. J. McDougall, and J. C. McWilliams (1995), Parameterizing eddy-induced tracer transports in ocean circulation models, *J. Phys. Oceanogr.*, *25*, 463–474.

Gill, A. E. (1982), *Atmosphere-Ocean Dynamics*, 662 pp., Elsevier, New York.

Gong, D., and S. Wang (1999), Definition of Antarctic Oscillation index, *Geophys. Res. Lett.*, *26*, 459–462.

Griffies, S. M. (1998), The Gent-McWilliams skew flux, *J. Phys. Oceanogr.*, *28*, 831–841.
Griffies, S. M., et al. (2005), Formulation of an ocean model for global climate simulations, *Ocean Sci.*, *1*, 45–79.
Hall, A., and M. Visbeck (2002), Synchronous variability in the Southern Hemisphere atmosphere, sea ice, and ocean resulting from the annular mode, *J. Clim.*, *15*, 3043–3057.
Hallberg, R., and A. Gnanadesikan (2006), The role of eddies in determining the structure and response of the wind-driven Southern Hemisphere overturning: Results from the Modeling Eddies in the Southern Ocean (MESO) project, *J. Phys. Oceanogr.*, *36*, 2232–2252, doi:10.1175/JPO2980.1.
Hughes, C. W., and B. A. de Cuevas (2001), Why western boundary currents in realistic oceans are inviscid: A link between form stress and bottom pressure torques, *J. Phys. Oceanogr.*, *31*, 2871–2885.
Hughes, C. W., P. L. Woodworth, M. P. Meredith, V. Stepanov, T. Whitworth, and A. R. Pyne (2003), Coherence of Antarctic sea levels, Southern Hemisphere Annular Mode, and flow through Drake Passage, *Geophys. Res. Lett.*, *30*(9), 1464, doi:10.1029/2003GL017240.
Intergovernmental Panel on Climate Change (IPCC) (2001), *Climate Change* 2001*: The Scientific Basis: Contribution of Working Group I to the Third Assessment Report of the Intergovernmental Panel on Climate Change*, edited by J. T. Houghton et al., 881 pp., Cambridge Univ. Press, New York.
Intergovernmental Panel on Climate Change (IPCC) (2007), *Climate Change* 2007*: The Physical Science Basis: Working Group I Contribution to the Fourth Assessment Report of the IPCC*, edited by S. Solomon et al., Cambridge Univ. Press, New York.
Large, W. G., and A. J. G. Nurser (2001), Ocean surface water mass transformation, in *Ocean Circulation and Climate: Observing and Modelling the Global Ocean*, *Int. Geophys. Ser.*, vol. 77, edited by G. Siedler, J. Church, and J. Gould, pp. 317–336, Academic, New York.
Le Quéré, C., et al. (2007), Saturation of the Southern Ocean CO_2 sink due to recent climate change, *Science*, *316*, 1735–1738.
Marshall, G. J. (2003), Trends in the Southern Annular Mode from observations and reanalyses, *J. Clim.*, *16*, 4134–4143.
Marshall, J., and T. Radko (2003), Residual-mean solutions for the Antarctic Circumpolar Current and its associated overturning circulation, *J. Phys. Oceanogr.*, *33*, 2341–2354.
Meredith, M. P., and A. M. Hogg (2006), Circumpolar response of Southern Ocean eddy activity to a change in the Southern Annular Mode, *Geophys. Res. Lett.*, *33*, L16608, doi:10.1029/2006GL026499.
Meredith, M. P., P. L. Woodworth, C. W. Hughes, and V. Stepanov (2004), Changes in the ocean transport through Drake Passage during the 1980s and 1990s, forced by changes in the Southern Annular Mode, *Geophys. Res. Lett.*, *31*, L21305, doi:10.1029/2004GL021169.
Miller, R. L., G. A. Schmidt, and D. T. Shindell (2006), Forced annular variations in the 20th century Intergovernmental Panel on Climate Change Fourth Assessment Report models, *J. Geophys. Res.*, *111*, D18101, doi:10.1029/2005JD006323.
Oke, P. R., and M. H. England (2004), Oceanic response to changes in the latitude of the Southern Hemisphere subpolar westerly winds, *J. Clim.*, *17*, 1040–1054.
Olbers, D., D. Borowski, C. Völker, and J.-O. Wölff (2004), The dynamical balance, transport and circulation of the Antarctic Circumpolar Current, *Antarct. Sci.*, *16*, 439–470.
Rintoul, S. R., and S. Sokolov (2001), Baroclinic transport variability of the Antarctic Circumpolar Current south of Australia (WOCE repeat section SR3), *J. Geophys. Res.*, *106*, 2815–2832.
Rintoul, S. R., C. W. Hughes, and D. Olbers (2001), The Antarctic Circumpolar Current system, in *Ocean Circulation and Climate: Observing and Modelling the Global Ocean*, *Int. Geophys. Ser.*, vol. 77, edited by G. Siedler, J. Church, and J. Gould, pp. 271–302, Academic, New York.
Russell, J. L., R. J. Stouffer, and K. W. Dixon (2006), Intercomparison of the Southern Ocean circulations in IPCC coupled model control simulations, *J. Clim.*, *19*, 4560–4575.
Sabine, C. L., et al. (2004), The oceanic sink for anthropogenic CO_2, *Science*, *305*, 367–371, doi:10.1126/science.1097403.
Saenko, O. A., J. C. Fyfe, and M. H. England (2005), On the response of the oceanic wind-driven circulation to atmospheric CO_2 increase, *Clim. Dyn.*, *25*, 415–426, doi:10.1007/s00382-005-0032-5.
Sen Gupta, A., and M. H. England (2006), Coupled ocean-atmosphere-ice response to variations in the Southern Annular Mode, *J. Clim.*, *19*, 4457–4486.
Sen Gupta, A., A. Santoso, A. S. Taschetto, C. C. Ummenhofer, J. Trevena, and M. H. England (2009), Projected changes to the Southern Hemisphere ocean and sea ice in the IPCC AR4 climate models, *J. Clim.*, *22*, 3047–3078.
Stouffer, R. J., J. Russell, and M. J. Spelman (2006), Importance of oceanic heat uptake in transient climate change, *Geophys. Res. Lett.*, *33*, L17704, doi:10.1029/2006GL027242.
Toggweiler, J. R., and B. Samuels (1995), Effect of Drake Passage on the global thermohaline circulation, *Deep Sea Res. Part I*, *42*, 477–500.
Treguier, A. M., I. M. Held, and V. D. Larichev (1997), Parameterization of quasigeostrophic eddies in primitive equation ocean models, *J. Phys. Oceanogr.*, *27*, 567–580.
Visbeck, M., J. Marshall, T. Haine, and M. Spall (1997), Specification of eddy transfer coefficients in coarse-resolution ocean circulation models, *J. Phys. Oceanogr.*, *27*, 381–402.
Wells, N. C., and B. A. de Cuevas (1995), Depth-integrated vorticity budget of the Southern Ocean from a general circulation model, *J. Phys. Oceanogr.*, *25*, 2569–2582.
Wright, D. K. (1997), A new eddy mixing parametrization and ocean general circulation model, *Int. WOCE Newsl.*, *26*, 27–29.

T. Kuhlbrodt, Department of Meteorology, NCAS-Climate, PO Box 243, Earley Gate, Reading RG6 6BB, UK. (t.kuhlbrodt@reading.ac.uk)
M. P. Meredith and Z. Wang, British Antarctic Survey, High Cross, Madingley Road, Cambridge CB3 0ET, UK. (zwa@bas.ac.uk)